Biosensors and Bioelectronics 41 (2013) 103–109

Contents lists available at SciVerse ScienceDirect

Biosensors and Bioelectronics

journal homepage: www.elsevier.com/locate/bios

Label-free detection of DNA hybridization using transistors based on CVD grown graphene

Tzu-Yin Chen [a,1], Phan Thi Kim Loan [b,1], Chang-Lung Hsu [b], Yi-Hsien Lee [a], Jacob Tse-Wei Wang [a], Kung-Hwa Wei [b], Cheng-Te Lin [a,*], Lain-Jong Li [a]

[a] Institute of Atomic and Molecular Sciences, Academia Sinica, Taipei 10617, Taiwan
[b] Department of Material Science and Engineering, National Chiao Tung University, Hsinchu 30010, Taiwan

ARTICLE INFO

Article history:
Received 2 June 2012
Received in revised form
25 July 2012
Accepted 26 July 2012
Available online 17 August 2012

Keywords:
Label-free detection
Liquid-gated transistors
DNA sensing
CVD graphene
Gold-transfer method

ABSTRACT

The high transconductance and low noise of graphene-based field-effect transistors based on large-area monolayer graphene produced by chemical vapor deposition are used for label-free electrical detection of DNA hybridization. The gate materials, buffer concentration and surface condition of graphene have been optimized to achieve the DNA detection sensitivity as low as 1 pM (10^{-12} M), which is more sensitive than the existing report based on few-layer graphene. The graphene films obtained using conventional PMMA-assisted transfer technique exhibits PMMA residues, which degrade the sensing performance of graphene. We have demonstrated that the sensing performance of the graphene samples prepared by gold-transfer is largely enhanced (by 125%).

1. Introduction

Exploring the interaction between deoxyribonucleic acids (DNA) and nanomaterials is helpful for developing biosensors. The development of nanomaterials for DNA detection such as inorganic nanoparticles (Drummond et al., 2003; Zhang et al., 2007), silicon nanowires (Patolsky and Lieber, 2005; Xie et al., 2012), nanoporous membranes (Li et al., 2003), and nanocarbon materials (Li et al., 2011; Muller et al., 2010; Schrand et al., 2009) is growing rapidly over the past few years. The majority of DNA detection technology has relied on optical or electrochemical transductions; however, these methods require fluorescent or electrochemical tags. Label-free electrical detection is considered as a candidate for development of cost-effective and sequence-selective DNA sensors. Carbon nanotube transistors show great promise in detecting ATP (Huang et al., 2009), DNAs (Gui et al., 2006; Tang et al., 2006; Dong et al., 2008; Fu et al., 2010; Sorgenfrei et al., 2011), proteins (Byon and Choi, 2006), and bacteria (Villamizar et al., 2008) on account of the high sensitivity and specificity. However, recent studies have revealed the potential cytotoxicity and genotoxicity of carbon nanotubes at the cellular level (Zhu et al., 2007; Allen et al., 2007). Another issue for carbon nanotubes is the coexistence of metallic and semiconducting carbon nanotubes in available ensembles, and it is of great challenge to obtain pure metallic or semiconducting nanotubes for the fabrication of field-effect transistors (FETs). An attractive alternative nanocarbon, graphene, has found fascinating applications in biosensor technology because of its large surface area and pronounced ambipolar characteristics (Fu and Li, 2010). Due to its atom-thick nature, the electrical properties of graphene are highly sensitive to the interaction between graphene surface and adsorbed foreign molecules. Graphene FETs fabricated with mechanically-exfoliated graphene or reduced graphene oxide have been used in the recognition of proteins (Ohno et al., 2009), bacteria (Mohanty and Berry, 2008), and single-stranded DNAs (Lin et al., 2010). However, the size of reduced graphene oxide is small ($\approx$ hundreds nanometers) and the electrical properties significantly vary with the preparation conditions (Su et al., 2009). In contrast, large-area single-layer graphene films grown by chemical vapor deposition (CVD) are more favorable for device fabrication, since the CVD process exhibits better reproducibility compared to the chemical exfoliation process (Li et al., 2009; Reina et al., 2009; Chen et al., 2012).

Detection of DNA molecules in dry state by bottom-gated graphene FETs have been reported, where DNAs act as negative potential gating agents (Lin et al., 2010; Lu et al., 2010). In these devices, the transfer characteristics show resistor-like behaviors (very small on/off current ratio), which can be attributed to the low gate coupling efficiency and the gapless feature of graphene.

* Corresponding author. Tel.: +886 2 23668205; fax: +886 2 23624957.
E-mail address: chengte.lin@gmail.com (C.-T. Lin).
[1] These authors contribute equally.

0956-5663/$ - see front matter © 2012 Elsevier B.V. All rights reserved.
http://dx.doi.org/10.1016/j.bios.2012.07.059

In this respect, our previous results indicated that label-free detection of DNA hybridization can be accomplished using liquid-gated FETs with few-layer graphene sheets prepared by CVD (Dong et al., 2010). The high transconductance and low noise of graphene FETs operated in liquid gating mode make them more attractive for biosensing purposes. So far, the interaction between biomolecules and graphene in aqueous solutions is still not fully understood. This may be figured out by examining the ambipolar characteristics of FETs in details because it is strongly related to graphene/electrolyte interface properties. In this study, we constructed liquid-gated FETs based on single-layer CVD graphene. The transfer curve change upon DNA immobilization and hybridization under various environments are investigated. These devices can achieve high sensitivity to detect as low as 1 pM (10^{-12} M) of target DNA. Meanwhile, the material of gate wires, the concentration of buffer solution, and the surface condition of graphene would obviously affect the sensing performance and surface charge state of the devices. The results shown in this contribution provide better understanding and useful information for the design of graphene-based DNA sensors.

2. Material and methods

2.1. Preparation and transfer of CVD graphene

Centimeter-scale graphene films were grown by CVD on 25 μm copper foils (Alfa Aesar, item no. 13382, purity 99.8%). The tube furnace was preheated to 1000 °C under H_2 flow to remove the native oxide of copper, and then a mixture of 60 sccm CH_4 and 15 sccm H_2 was introduced into the system to grow graphene. A transfer process was carried out to separate graphene from the foil by dissolution of Cu and put on insulating substrates using poly(methyl methacrylate) (MicroChem, PMMA 950K A4) as a capping layer. Firstly, PMMA was spin-coated on graphene/copper sheets, and then copper was etched in ferric nitrate solution (50 g/L, J.T.Baker ACS reagent, 98.0%). A transparent PMMA/graphene thin film can be obtained after removal of copper and cleaning. The films were transferred onto SiO_2 (300 nm)/Si substrate, and PMMA was dissolved in hot acetone (60 °C) overnight. In order to ensure no PMMA remained on the surface, graphene films were annealed at 450 °C in a mixed atmosphere (H_2: 20 sccm + Ar: 80 sccm) to decompose the polymers.

2.2. Transistor fabrication and characterizations

For device fabrication, silver paint (PELCO®, item no. 16034) was spread onto graphene films with 1 × 1 cm in area set on SiO_2 (300 nm)/Si substrate to make source and drain electrodes with diameter of 3 mm. The source and drain electrodes were protected from solution by covering with silicone rubber (Dow Corning® 3140) and a reservoir (8 × 8 mm in area) was also built in the same way to hold electrolyte. The test solutions were dropped on the surface of graphene from a micropipette and kept in silicone rubber reservoir. The size of the whole device is 1.5 × 1.5 cm. Silver, graphite, and platinum wires (diameter: 1 mm) were used as the gate electrode, respectively. Single-stranded DNA molecules (Sigma Aldrich) with the sequences: 5′–AGG TCG CCG CCC-3′ (as probe) and 3′–TCC AGC GGC GGG-5′ (as complement "target") were tested. DNAs were dissolved to different concentrations in phosphate buffered saline (PBS, Uni-Region Bio-Tech). The composition of 10 × PBS is 1370 mM NaCl, 27 mM KCl, 43 mM Na_2HPO_4, and 14.7 mM KH_2PO_4.

The transfer characteristics of liquid-gated graphene FETs were measured by semiconductor parameter analyzer (Keithley, Model 4200-SCS). The liquid-gate voltage was controlled in a relatively narrow range to avoid any side effects. Atomic force microscopy (AFM) images were taken by Veeco Dimension-Icon system. The quality of graphene films were determined by confocal Raman microscopic system (NT-MDT, laser wavelength: 473 nm, laser power: 0.5 mW, spot size: ≈0.5 μm). Silicon peak at 520 cm^{-1} was utilized as reference for wavenumber calibration.

3. Results and discussions

3.1. Configuration of liquid-gated graphene FETs

Single-layer CVD graphene was grown on copper foils at 1000 °C using CH_4/H_2 gases as described elsewhere (Su et al., 2011; Lu et al., 2012). The graphene/Cu foil films were spin-coated with a supporting layer of PMMA, followed by etching Cu in $Fe(NO_3)_2$ solution. The PMMA-supported graphene was then transferred onto insulating substrates, followed by removal of PMMA using acetone. The inset of Fig. 1a shows a photograph of a graphene sheet with 1 cm^2 in area set on SiO_2 (300 nm)/Si substrate. In Fig. 1a, Raman spectrum for as-transferred sample exhibits features of high-quality single-layer graphene: a symmetric 2D-band (≈2700 cm^{-1}) with a full width at half maximum of 30.2 cm^{-1} and a high I_{2D}/I_G ratio (1.95) (Li et al., 2009; Reina et al., 2009). After thermal cleaning in H_2/Ar environment (20/80 sccm) at 450 °C, a blue shift in G-band (from 1588.6 to 1592.0 cm^{-1}) and 2D-band (from 2701.9 to 2716.9 cm^{-1}) occurs, indicating that graphene is *p*-doped by annealing (Ryu et al., 2010). Some defects may be introduced to graphene by thermal treatment, resulting in the appearance of a weak D-band (at 1361.5 cm^{-1}) for the annealed sample.

The configuration of our graphene device is schematically shown in Fig. 1b. The liquid-gated FETs are fabricated by forming source and drain electrodes on graphene using silver paste. The silicone rubber is applied to cover the electrodes for the isolation of electrodes and solutions, and an external conducting wire is employed as a gate electrode. The conductance between source and drain varies in response to the surface electric potential of graphene. And the gate electrode coupled through the liquid electrolytes is used to control the on and off switching of the devices (Patolsky et al., 2006). The transfer curves (drain current I_d versus gate voltage V_g) of the liquid-gated FETs with as-transferred and annealed graphene films are recorded in phosphate buffered saline (PBS) solutions. In Fig. 1c ambipolar characteristics can be clearly observed when a small range of gate voltage (from −0.1 to 0.8 V) is applied to the solution. The charge neutrality point (V_{CNP}: the applied gate voltage corresponding to the minimum conductance) of the devices made of as-transferred and annealed graphene are at $V_g = 0.21$ and 0.52 V, respectively. The right shift of V_{CNP} confirms the observation in Fig. 1a that the carrier density of graphene is increased (*p*-doped) after annealing.

3.2. Effect of gate materials

The gate electrodes made from different materials are examined. Fig. 2a compares the transfer curves of a graphene FET operated with various gate electrodes. When a device is gated by a silver wire, natural graphite needle, and platinum filament, their V_{CNP} are 0.12, 0.20, and 0.94 V, respectively. The applied V_g makes free mobile ions in PBS form an electrostatic double layer between graphene and electrolytes. The electrostatic double layer works as a top-gate dielectric layer ranging from a few angstroms to several nanometers in thickness described by the Debye–Hückel equation (Ohno et al., 2009). The potential across electrostatic double layer and graphene is determined by V_g and the interface voltage between gate electrode and electrolytes. Since the work function value is determined by the material used, the

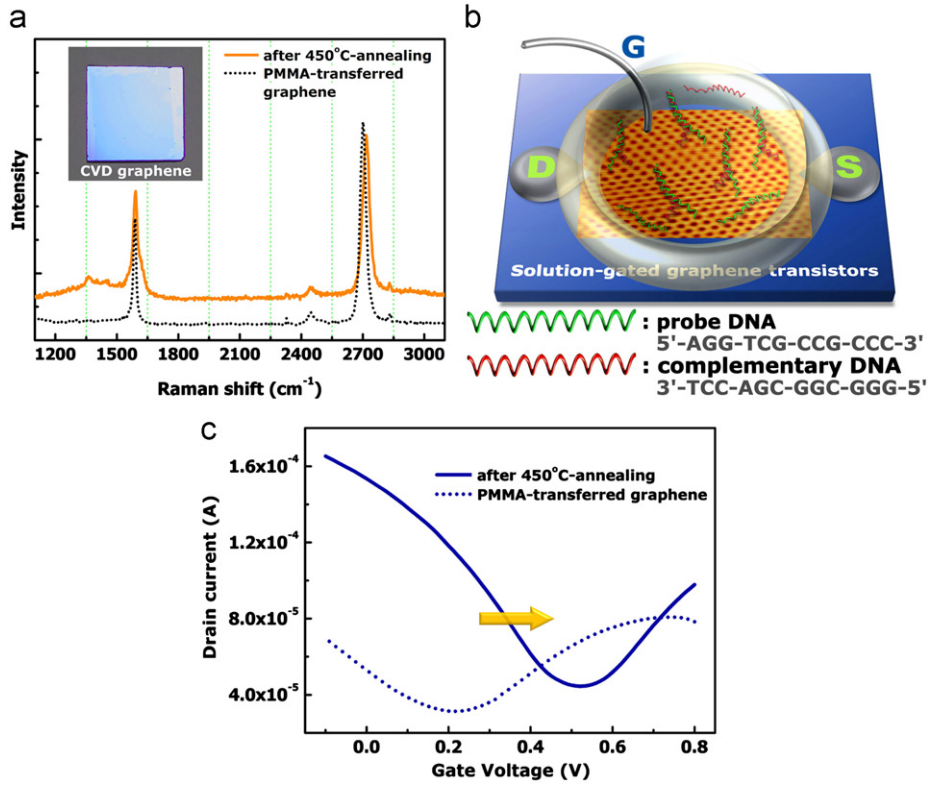

Fig. 1. (a) Raman spectra of single-layer CVD graphene before and after thermal cleaning. The inset shows a graphene sheet set on silicon substrate. (b) Schematic illustration of a graphene FET in liquid-gated configuration. (c) Transfer curves of a liquid-gated graphene FET before and after annealing.

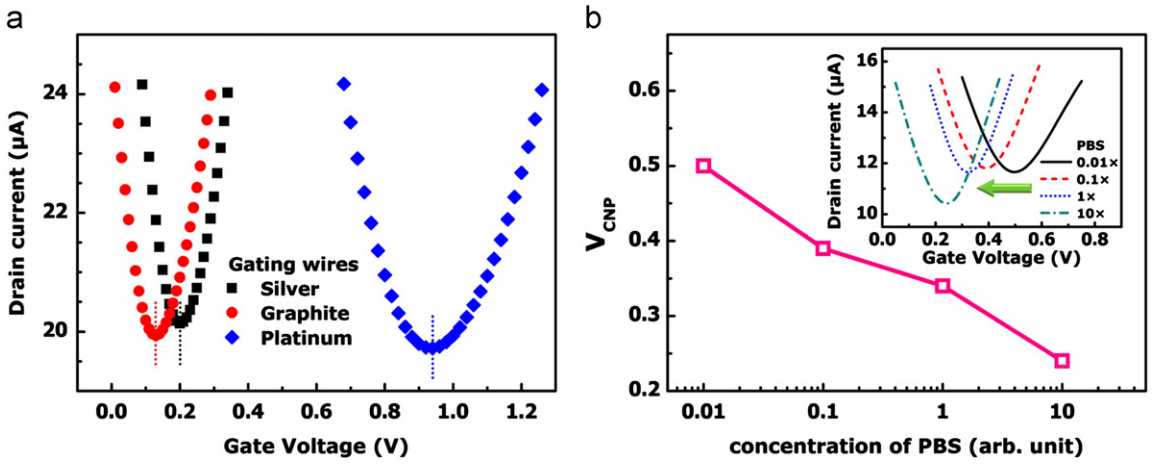

Fig. 2. (a) Transfer curves of the graphene FET operated with various gate electrodes. (b) The V_{CNP} position of a graphene device determined in different concentrations of PBS buffer solution. The inset shows the transfer characteristics obtained in $0.01\times \sim 10\times$ PBS.

interface voltage in each case is also different, resulting in various V_{CNP} (Minot et al., 2007). As a result, platinum filament is not preferred as gate electrode due to the fact that V_{CNP} is too high, which may cause large gate leakage and significant crowding of counter-ions on graphene surface (Miskovic and Upadhyaya, 2010). And the graphite needles may generate undesirable electrochemical reactions at the exposed graphene edges (Kim et al., 2006). Therefore, silver wire electrode (diameter: 1.0 mm) is better for DNA detection and it is adopted for subsequent studies.

3.3. *Effect of PBS buffer solutions*

It is known that both the content and the concentration of electrolytes can significantly affect the performance of solution-gated graphene FETs (Chen et al., 2009b,c). In this study, PBS is employed as a buffer solution for DNA hybridization analysis. The graphene films used here were synthesized on Cu foils by CVD and transferred to desired substrates by PMMA, followed by acetone wash and thermal annealing as described in experimental section. The inset in Fig. 2b presents the transfer characteristics of a graphene device obtained in different PBS concentrations ($0.01\times -10\times$). As shown in Fig. 2b, the linear dependence of V_{CNP} versus buffer concentration indicates that large positive V_{CNP} could be obtained in diluted PBS. Because the negatively-charged impurities originated from the transfer process or SiO_2 substrates are trapped underneath graphene layer, it leads to intrinsic *p*-type behavior in graphene FETs (Shi et al., 2009). As PBS concentration increases, more positive ions are attracted to the device surface, naturalizing

the trapped negative charges and generating the left shift of V_{CNP} (Chen et al., 2009b).

The influence of PBS concentration on the sensing performance of target DNA hybridized with probe DNA-decorated graphene FETs was further investigated. The 12-mer probe and target DNA strands were respectively dissolved in 10 ×, 1 ×, and 0.1 × PBS solutions. In each round of the experiment, the first transfer curve was taken after immersing the devices in pure PBS for 2 h. The probe DNA solution (10 μm) was then added in the chamber and incubated for 16 h to achieve the saturation adsorption on graphene, then followed by a rinsing process to remove weakly-bound DNAs. Target DNAs were added to the probe DNA-immobilized devices for hybridization. After 4 h, the samples were rinsed and measured for the transfer characteristics in fresh PBS. Note that the interaction between probe and target DNA molecules is strong, thus the hybridized target DNAs cannot be simply removed by rinsing at room temperature. Hence, the detection experiments for target DNA molecules from low to high concentrations were carried out in sequence. As shown in Fig. 3a–c, the V_{CNP} shifts toward negative gate bias as the concentration of target DNAs is increased. It is noted that the negative shift in threshold voltage of carbon nanotube FETs upon DNA hybridization has also been observed and the DNA strands are considered to impose *n*-doping to the nanotubes (Star et al., 2006; Gui et al., 2007). It has been naturally speculated that hybridized DNA molecules cause *n*-doping in graphene (Dong et al., 2010). The negative shift may be related to the interaction between graphene and electron-rich nucleobases in DNA molecules (Ortmann et al., 2005; Manohar et al., 2008). Notice that the direction of V_{CNP} shift upon the addition of target DNA is independent of PBS concentration.

In Fig. 3a–c, the transfer curves of the devices before immobilization of DNAs (black solid lines) reveal that V_{CNP} are at V_g=0.29 (10 ×), 0.40 (1 ×), and 0.50 V (0.1 × PBS), respectively. This agrees with the observations in Fig. 2b. Interestingly, upon raising the concentration of added target DNAs, the slope of *p*- and *n*-channels in the transfer curves decreases when FETs were operated in 0.1 × PBS, indicating the decrease of both electron and hole mobility. Whereas the slope of transfer curves for both *p*- and *n*-channels is almost constant in 10 × PBS solutions. At a higher ionic concentration the screening effect becomes strong, which minimizes the charge impurity scattering caused by adsorbed DNA molecules (Adam et al., 2007; Chen et al., 2009a). In addition, asymmetric curves are observed in Fig. 3c (0.1 × PBS), which are due to the fact that the scattering strength of the charged impurities is different for holes and electrons (Novikov, 2007; Zhang and Li, 2010).

The single-layer graphene FETs show superior sensing performance than that made of few-layer graphene layers. The sensitivity of our samples can achieve as low as 1 pM for DNA detection, whereas the detection limit is 10 pM when using few-layer graphene devices (Dong et al., 2010). Under the same conditions (1 × PBS and 10 nM target DNA hybridized), the V_{CNP} shift of single-layer graphene FETs is 140% enhanced than that of few-layer samples. Meanwhile, Fig. 3d compares the sensing sensitivity of DNA hybridization in varied PBS concentration. The results show that the lower PBS concentration results in higher detection sensitivity, i.e. larger shift in V_{CNP}. It is noteworthy that in order

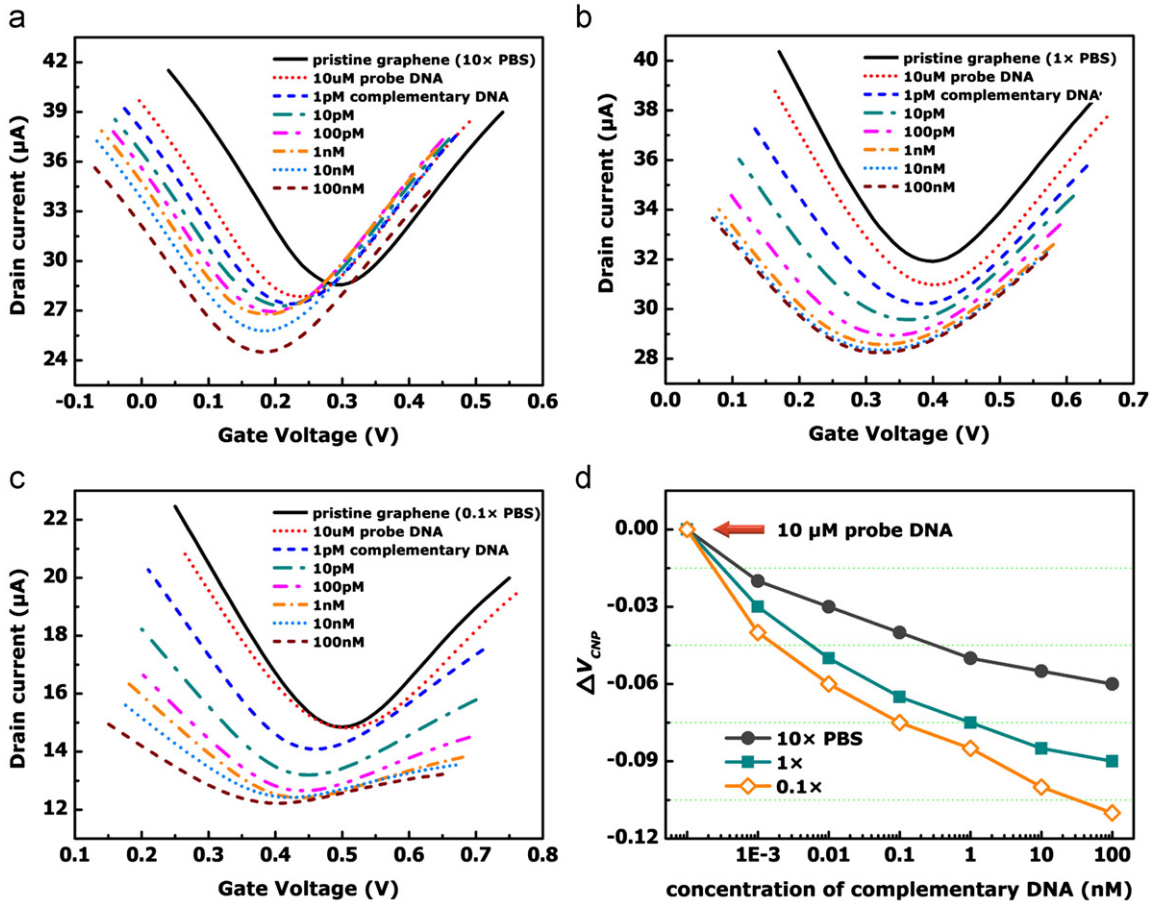

Fig. 3. Transfer characteristics of probe DNA pre-immobilized graphene FETs hybridizing with target DNAs, which were added from 1 pM to 100 nM in sequence. The devices were measured in (a) 10 ×; (b) 1 ×; (c) 0.1 × PBS, respectively. (d) A summary of V_{CNP} shift of the devices shown in (a–c). The V_{CNP} as a function of the concentration of added target DNAs, where V_{CNP} of probe DNA decorated graphene is also included.

to have enough electrical responses from liquid-gated graphene with DNA attachment, a lower buffer concentration (i.e. lower capacitance of electrostatic double layer) should be used. However, a very low PBS concentration shifts the neutrality point to a more positive position becomes unfavorable for solution gating operation. Therefore, the selection of an intermediate PBS concentration about 1 × is appropriate and this concentration is also close to biological conditions.

3.4. Effect of graphene surfaces

To investigate the effect of graphene surface condition to the DNA sensing performance, the commonly used PMMA layer (as a graphene transfer supporting layer) is replaced by a layer of Au film, where the Au layer can be easily removed by a gold etcher (KI+Iodine). Note that the gold-transferred samples are directly employed as sensing layer without the need to use post-thermal treatment to clean up the surfaces. The Raman spectra Fig. 4a shows that both gold-transferred graphene and annealed PMMA-graphene exhibit a G-band at 1595.7 and 1591.7 cm^{-1} in addition to 2D-band at 2719.8 and 2720.3 cm^{-1} correspondingly. The I_{2D}/I_G ratio of the gold-transferred sample (1.81) is comparable to that (1.58) of the annealed PMMA one. Fig. 1a suggests that the graphene transferred by PMMA and Au are comparable in film quality. However, the morphology of these two films is significantly different. The graphene transferred using PMMA is known to have a very thin layer of PMMA residues on the surface (Dan et al., 2009). It can be found in Fig. 4b that the graphene layer is still covered with some PMMA residues even after annealing. In clear contrast, the surface of the gold-transferred graphene is relatively much cleaner, as demonstrated in Fig. 4c.

Fig. 5a–c display the sensing behaviors for three types of graphene devices, including (a) annealed PMMA-graphene, (b) gold-transferred graphene, and (c) sample (a) with an additional PMMA coating (≈ 120 nm) on top. Note that the purpose of the sample c is to amplify the effect of PMMA on graphene surfaces. In Fig. 5d, it is clearly seen that the V_{CNP} shift is larger for Au-transferred graphene FET. And the graphene coated with a thin layer of PMMA shows worse sensing performance since the interaction between graphene and DNA is blocked by PMMA coating. These results suggest that DNA interaction with graphene is strongly affected by the cleanness of graphene surface. It also indicates that PMMA residues remaining on commonly used CVD graphene degrades the sensing performance of the device. Hence, a cleaner transfer technique such as Au-transfer is required for enhancing the sensitivity of graphene sensors.

4. Conclusions

The label-free electrical detection of DNA hybridization using liquid-gated, single-layer CVD graphene is demonstrated and the DNA detection sensitivity for our graphene devices can achieve the concentration as low as 1 pM (10^{-12} M). It is also investigated

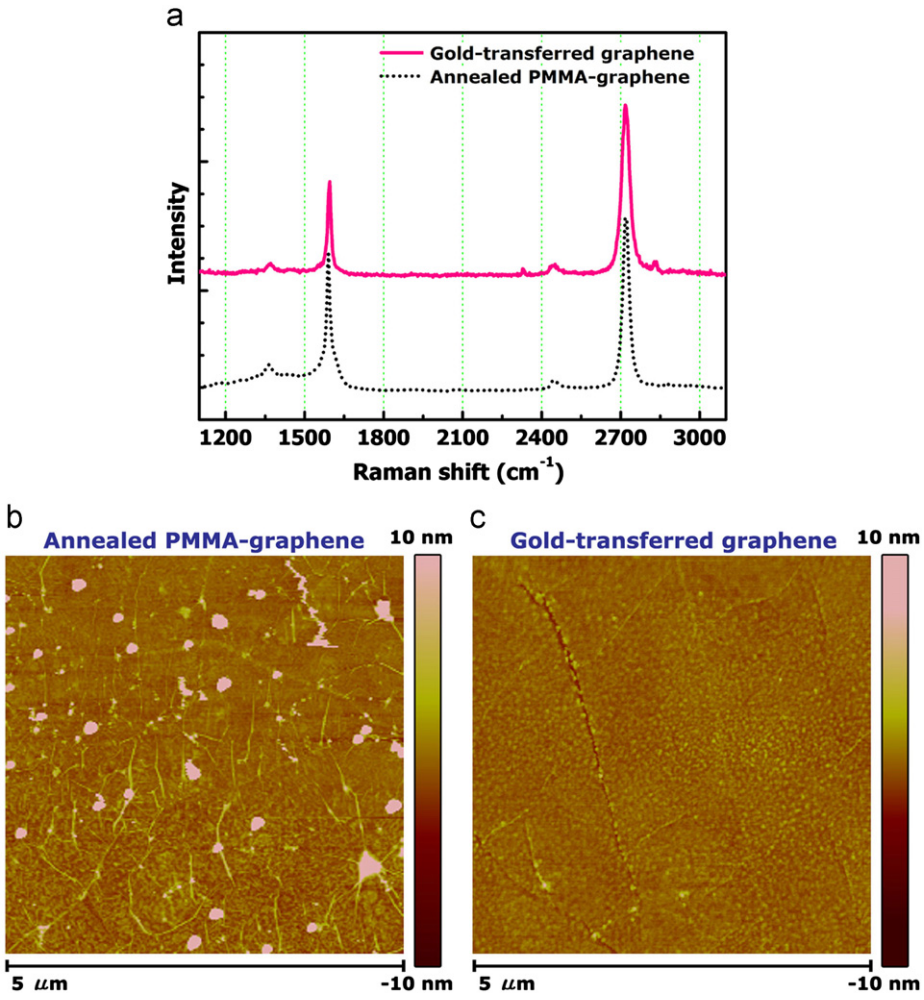

Fig. 4. (a) Raman spectra of graphene sheets prepared by gold-transfer and PMMA-transfer methods, respectively. (b) (c) AFM images of PMMA- and gold-transferred graphene. Note that annealing was performed for PMMA-transferred sample.

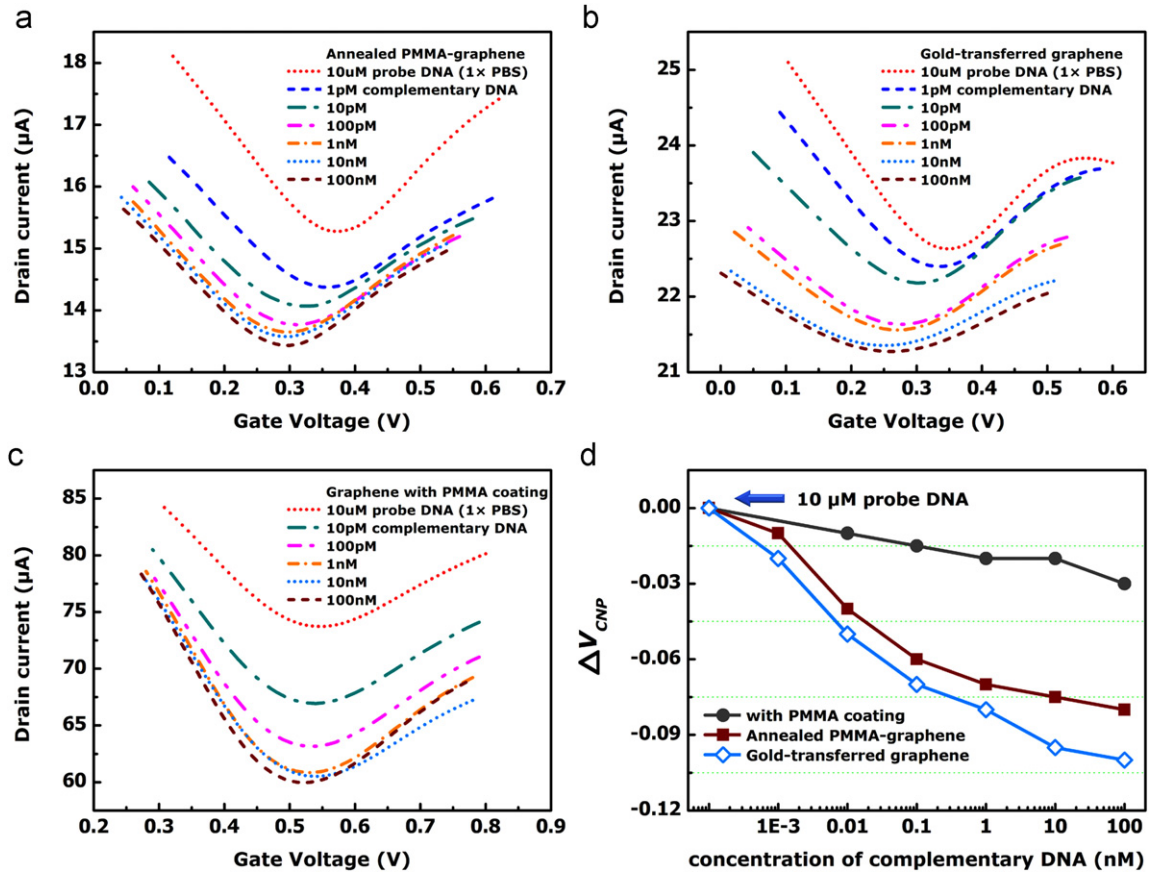

Fig. 5. DNA detection using graphene FETs with different surface conditions: (a) PMMA-transferred graphene after thermal cleaning; (b) gold-transferred graphene; and (c) sample (a) with an additional PMMA coating (≈ 120 nm). (d) A summary of V_{CNP} shift of the devices shown in (a–c). The graphene with cleaner surface exhibits superior sensing performance (larger shift in V_{CNP}).

that the interaction between DNA and graphene is strongly affected by the cleanness of graphene surface. The graphene films obtained using conventional PMMA-assisted transfer technique exhibits PMMA residues, unavoidably degrading the sensing performance of graphene. We have demonstrated that the sensing performance of the graphene samples prepared by gold-transfer is largely enhanced (by 125%). This report has focused on the sensing of short chain DNA hybridization, and the studies for longer chain DNA or protein molecules are worthy of more investigations. Meanwhile, this report may stimulate further developments in graphene transfer techniques as well as studies on the surface interaction between graphene and organic polymer or biomolecules.

Acknowledgments

This research was supported by National Science Council Taiwan (NSC-99-2112-M-001-021-MY3 and 99-2738-M-001-001) and Academia Sinica (IAMS and Nano program). We also acknowledge the support from NCTU Taiwan.

References

Adam, S., Hwang, E.H., Galitski, V.M., Das Sarma, S., 2007. Proceedings of the National Academy of Sciences of the United States of America 104, 18392–18397.
Allen, B.L., Kichambare, P.D., Star, A., 2007. Advanced Materials (Weinheim, Germany) 19, 1439–1451.
Byon, H.R., Choi, H.C., 2006. Journal of the American Chemical Society 128, 2188–2189.
Chen, C.-H., Lin, C.-T., Lee, Y.-H., Liu, K.-K., Su, C.-Y., Zhang, W., Li, L.-J., 2012. Small (Weinheim an der Bergstrasse, Germany) 8, 43–46.
Chen, F., Xia, J.L., Tao, N.J., 2009a. Nano Letters 9, 1621–1625.
Chen, F., Xia, J.L., Ferry, D.K., Tao, N.J., 2009b. Nano Letters 9, 2571–2574.
Chen, F., Qing, Q., Xia, J.L., Li, J.H., Tao, N.J., 2009c. Journal of the American Chemical Society 131, 9908–9909.
Dan, Y.P., Lu, Y., Kybert, N.J., Luo, Z.T., Johnson, A.T.C., 2009. Nano Letters 9, 1472–1475.
Dong, X.C., Shi, Y.M., Huang, W., Chen, P., Li, L.J., 2010. Advanced Materials (Weinheim, Germany) 22, 1649–1653.
Dong, X.C., Fu, D.L., Xu, Y.P., Wei, J.Q., Shi, Y.M., Chen, P., Li, L.J., 2008. Journal of Physical Chemistry C 112, 9891–9895.
Drummond, T.G., Hill, M.G., Barton, J.K., 2003. Nature Biotechnology 21, 1192–1199.
Fu, D.L., Li, L.J., 2010. Nano Reviews 1, 5354.
Fu, D.L., Okimoto, H., Lee, C.W., Takenobu, T., Iwasa, Y., Kataura, H., Li, L.J., 2010. Advanced Materials (Weinheim, Germany) 22, 4867–4871.
Gui, E.L., Li, L.J., Lee, P.S., Lohani, A., Mhaisalkar, S.G., Cao, Q., Kang, S.J., Rogers, J.A., Tansil, N.C., Gao, Z.Q., 2006. Applied Physics Letters 89, 232104.
Gui, E.L., Li, L.J., Zhang, K.K., Xu, Y.P., Dong, X.C., Ho, X.N., Lee, P.S., Kasim, J., Shen, Z.X., Rogers, J.A., Mhaisalkar, S.G., 2007. Journal of the American Chemical Society 129, 14427–14432.
Huang, Y.X., Sudibya, H.G., Fu, D.L., Xue, R.H., Dong, X.C., Li, L.J., Chen, P., 2009. Biosensors & Bioelectronics 24, 2716–2720.
Kim, T., Lim, S., Kwon, K., Hong, S.H., Qiao, W.M., Rhee, C.K., Yoon, S.H., Mochida, I., 2006. Langmuir: The ACS Journal of Surfaces and Colloids 22, 9086–9088.
Li, H.L., Zhang, Y.W., Luo, Y.L., Sun, X.P., 2011. Small (Weinheim an der Bergstrasse, Germany) 7, 1562–1568.
Li, J.L., Gershow, M., Stein, D., Brandin, E., Golovchenko, J.A., 2003. Nature Materials 2, 611–615.
Li, X.S., Cai, W.W., An, J.H., Kim, S., Nah, J., Yang, D.X., Piner, R., Velamakanni, A., Jung, I., Tutuc, E., Banerjee, S.K., Colombo, L., Ruoff, R.S., 2009. Science (New York, NY) 324, 1312–1314.
Lin, J.A., Teweldebrhan, D., Ashraf, K., Liu, G.X., Jing, X.Y., Yan, Z., Li, R., Ozkan, M., Lake, R.K., Balandin, A.A., Ozkan, C.S., 2010. Small (Weinheim an der Bergstrasse, Germany) 6, 1150–1155.
Lu, A.-Y., Wei, S.-Y., Wu, C.-Y., Hernandez, Y., Chen, T.-Y., Liu, T.-H., Pao, C.-W., Chen, F.-R., Li, L.-J., Juang, Z.-Y., 2012. RSC Advances 2, 3008–3013.
Lu, Y., Goldsmith, B.R., Kybert, N.J., Johnson, A.T.C., 2010. Applied Physics Letters 97, 083107.

Manohar, S., Mantz, A.R., Bancroft, K.E., Hui, C.Y., Jagota, A., Vezenov, D.V., 2008. Nano Letters 8, 4365–4372.
Minot, E.D., Janssens, A.M., Heller, I., Heering, H.A., Dekker, C., Lemay, S.G., 2007. Applied Physics Letters 91, 093507.
Miskovic, Z.L., Upadhyaya, N., 2010. Nanoscale Research Letters 5, 505–511.
Mohanty, N., Berry, V., 2008. Nano Letters 8, 4469–4476.
Muller, K., Malik, S., Richert, C., 2010. ACS Nano 4, 649–656.
Novikov, D.S., 2007. Applied Physics Letters 91, 102102.
Ohno, Y., Maehashi, K., Yamashiro, Y., Matsumoto, K., 2009. Nano Letters 9, 3318–3322.
Ortmann, F., Schmidt, W.G., Bechstedt, F., 2005. Physical Review Letters 95, 186101.
Patolsky, F., Lieber, C.M., 2005. Materials Today 8, 20–28.
Patolsky, F., Zheng, G.F., Lieber, C.M., 2006. Analytical Chemistry 78, 4260–4269.
Reina, A., Jia, X.T., Ho, J., Nezich, D., Son, H.B., Bulovic, V., Dresselhaus, M.S., Kong, J., 2009. Nano Letters 9, 30–35.
Ryu, S., Liu, L., Berciaud, S., Yu, Y.J., Liu, H.T., Kim, P., Flynn, G.W., Brus, L.E., 2010. Nano Letters 10, 4944–4951.
Schrand, A.M., Hens, S.A.C., Shenderova, O.A., 2009. Critical Reviews in Solid State and Materials Sciences 34, 18–74.
Shi, Y.M., Dong, X.C., Chen, P., Wang, J.L., Li, L.J., 2009. Physical Review B 79, 115402.
Sorgenfrei, S., Chiu, C.Y., Gonzalez, R.L., Yu, Y.J., Kim, P., Nuckolls, C., Shepard, K.L., 2011. Nature Nanotechnology 6, 125–131.
Star, A., Tu, E., Niemann, J., Gabriel, J.C.P., Joiner, C.S., Valcke, C., 2006. Proceedings of the National Academy of Sciences of the United States of America 103, 921–926.
Su, C.Y., Fu, D.L., Lu, A.Y., Liu, K.K., Xu, Y.P., Juang, Z.Y., Li, L.J., 2011. Nanotechnology 22, 185309.
Su, C.Y., Xu, Y.P., Zhang, W.J., Zhao, J.W., Tang, X.H., Tsai, C.H., Li, L.J., 2009. Chemistry of Materials: A Publication of the American Chemical Society 21, 5674–5680.
Tang, X.W., Bansaruntip, S., Nakayama, N., Yenilmez, E., Chang, Y.L., Wang, Q., 2006. Nano Letters 6, 1632–1636.
Villamizar, R.A., Maroto, A., Rius, F.X., Inza, I., Figueras, M.J., 2008. Biosensors & Bioelectronics 24, 279–283.
Xie, P., Xiong, Q.H., Fang, Y., Qing, Q., Lieber, C.M., 2012. Nature Nanotechnology 7, 119–125.
Zhang, J., Song, S.P., Wang, L.H., Pan, D., Fan, C.H., 2007. Nature Protocols 2, 2888–2895.
Zhang, W.J., Li, L.J., 2010. New Journal of Physics 12, 103037.
Zhu, L., Chang, D.W., Dai, L.M., Hong, Y.L., 2007. Nano Letters 7, 3592–3597.